
Article:
Cooper, E.J., Berrow, S.R., Margaryan, K. et al. (Accepted: 2026) Insight Into the Composition-Dependent Transition from Auxetic Nematic to Frustrated Smectic in Liquid Crystal Elastomers. Physical Review E. ISSN: 1539-3755 (In Press)

Insight Into the Composition-Dependent Transition from Auxetic Nematic to Frustrated Smectic in Liquid Crystal Elastomers

Emily J. Cooper,[1] Stuart R. Berrow,[1] Karine Margaryan[2], Gevorg Gevorgyan[2], Mariam Hakobyan[2], Thomas Raistrick,[1] Ethan I.L. Jull,[1] Devesh Mistry,[1] Peter Hine,[1] Aidan Street[1], Rafik Hakobyan[2], Helen F. Gleeson[1,*]

[1] School of Physics and Astronomy, University of Leeds, Leeds, U.K.

[2] Institute of Physics, Yerevan State University, Yerevan, Armenia

ORCiD: E.J. Cooper: 0009-0007-2440-2492, Stuart R. Berrow: 0000-0003-3764-1613, Gevorg Gevorgyan: 0000-0002-4500-1141, Thomas Raistrick: 0000-0002-6227-6550, Ethan I.L. Jull: 0000-0003-3228-1348, Devesh Mistry: 0000-0003-0012-6781, Helen F. Gleeson: 0000-0002-7494-2100.

ABSTRACT. The ability to optimise the properties of a material is particularly advantageous for applications. Here, the tuneable properties of side-chain liquid crystal elastomers (LCEs) are investigated. LCEs were fabricated using the same acrylate monomers, varying the proportion of mesogenic groups to influence the phase, density and mechanical properties. The density increases with mesogenic content, varying from 1.11 g/cm^3 to 1.19 g/cm^3 as the mesogenic content is increased from 51 mol% to 99 mol%. The 7% increase in density was attributed to closer packing of the nanoscale network, observed directly through Small- and Wide- Angle X-ray Scattering. A 22% reduction in the network end-to-end spacing was measured for LCEs as the mesogenic content was changed from 56 mol% to 75 mol%. LCEs with above 70 mol% mesogenic content were revealed to exhibit a frustrated smectic phase, with nematic phases confirmed for the lower mesogenic concentrations. The frustrated smectic materials exhibit a higher correlation length parallel to the director (> 125 Å) than the nematic LCEs (< 100 Å) and demonstrate significantly higher Young's moduli, with the greatest moduli perpendicular to the director measured at 21°C as 8.3 MPa for the smectic LCEs and as a constant value of 2.1 MPa for the nematic LCEs. Crucially, this demonstrates that only a small change in the mesogenic content can induce a transition from a nematic LCE to a frustrated smectic LCE. This series of materials reveals how the nanoscale packing, the macroscopic material properties, and the phase can be controlled *via* the mesogenic content in side-chain acrylate LCEs, suggesting design approaches that allow for the potential customisation of the material properties for applications.

I. INTRODUCTION

Liquid Crystal Elastomers (LCEs) are lightly crosslinked networks containing mesogenic components, which unite elastomeric behaviour with liquid crystallinity, resulting in extremely desirable and tuneable material properties. For example, some side chain LCEs, including those considered in this work, have been shown to be mechanical metamaterials on a molecular level, exhibiting negative Poisson's ratios above a material-dependent threshold strain [1-10]. Suggested applications of such LCEs include strain-controlled sub-micron diffraction gratings [5], multidimensional encryption and information storage [9], and impact resistance in glass [11]. More commonly, LCEs are main chain systems and properties such as the significant and reversible changes that occur at phase transitions have led to suggested uses as actuators in soft robotics [12,13], biomimetic and biological devices [14-17], sensors [18,19], and smart adhesives [20,21]. When considering the wide range of potential applications of LCEs, design rules are crucial to achieve the desired material behaviour and (often multiple) functionalities. As an example, for LCEs to be effective candidates for use as laminates within impact resistant glass, they must be both optically transparent and capable of effectively dissipating energy at ambient temperatures, features that have been demonstrated in some of the LCEs considered in this work [3-5,11].

There is a considerable body of research that has explored the role of composition on the properties of LCEs and liquid crystal networks (LCNs) *via* control of the crosslink density [8,22-25], the concentration of the mesogenic components [11,26], and the use of different mesogenic components [6,10,18,27,28]. The influence of compositional changes on the density of a material has also been considered for light-induced *cis-to-trans* isomerization in azobenzene-containing LCNs [29,30]. This paper considers systematic alterations to the composition of a side chain LCE, specifically varying the proportion of mesogenic groups and thus providing a fine control of the nanoscale network packing. We offer new insights into composition-related network packing and associated changes in the liquid crystal phase exhibited, as well as macroscopic material properties such as density and the Young's moduli. The design rules outlined in this paper build on the optical tunability that has already been demonstrated in this family of LCEs [11], but in addition demonstrate how small compositional

*Contact author: H.F.Gleeson@leeds.ac.uk

changes in LCEs can be used to change the phase and therefore mechanical behaviour [10].

Cooper *et al*. [11] demonstrated that small compositional changes of the family of LCEs also considered here offered a route for fine control of their refractive indices, and thus an approach for optimising optical transmission in applications such as laminates in impact resistance glass. In those materials two observations were made that suggested that the density of the LCE was dependant on composition rather than the liquid crystal phase: a linear decrease of the refractive indices observed between ~ 25°C and 55°C; and matching of the average refractive index for monodomain nematic and the chemically identical isotropic LCEs at the same temperature, (obeying the Newton mixing rules [31]). These observations offered the motivation for this more detailed study of the nanoscale and macroscopic properties of that family of LCEs.

In addition to exploring details of the influence of composition on the density of the LCEs, this paper considers its role on the nano-structure and phase of the resultant polymerized material. Berrow *et al.* [6] utilised X-ray scattering to characterize the monodomain nematic and smectic phases for a series of LCEs and they demonstrated that some materials exhibit bulk properties characteristic of nematic LCEs even though the phase assignation was 'smectic-like'. More recently, such 'smectic-like' materials have been identified as frustrated smectic LCEs, which occur when a nematic precursor forms a polymerized smectic LCE [10,28]. Frustrated smectic LCEs share some characteristics of monodomain nematic LCEs; in particular, they have been shown to have similar Young's moduli, some can be strained to more than 1.0, and some exhibit an auxetic response under strain [10,28]. The formation of frustrated smectic LCEs is considered in detail in [10] that smectic polymers templated in a nematic solvent, as is the case for this family of materials, were predicted by de Gennes to have very different mechanical properties from those formed in a smectic solvent. [40] This paper explores the composition-induced transition from nematic to frustrated smectic LCEs, describing the concomitant subtle changes in network packing and macroscopic properties.

II. METHODS

A. The Polymerized LCE Films

The fabrication of monodomain nematic, isotropic, and frustrated smectic LCEs has been described in detail in previous publications [1-11,18,21,25,28] and is also summarised in the Supplemental Material [32].

The LCE films studied are formed from both mesogenic and non-mesogenic acrylate monomers; the former include a crosslinker, 1,4-bis-[4-(6-acryloyloxyhexyloxy)benzoyloxy]-2-methylbenzene (RM82) and a monofunctional mesogenic side group, 6-(4-cyano-biphenyl-4'-yloxy)hexyl acrylate (A6OCB) while the latter is 2-ethylhexyl acrylate (EHA). The final films also include small quantities of the photoinitiator, methyl benzoylformate (MBF). The composition of the materials considered in this work is summarised in Table I. For LCEs between 51 mol% and 75 mol% mesogenic content, there is a systematic variation between the overall mesogenic content and the non-mesogenic content of the precursor mixture, with the ratio of RM82 and A6OCB in the polymerized LCE fixed (1:7). With this methodology, a large change in the mesogenic content of an LCE can be generated with very little change to the crosslinking density; increasing the mesogenic content from 51 mol% to 75 mol%, only changes the crosslink density from 6 mol% to 9 mol%. The materials with 98 mol% and 99 mol% of mesogens (i.e no EHA) have been described in detail by Jull *et al.* [25]; they are networks (LCNs) rather than elastomers, with glass transition temperatures of ~ 57°C and ~ 46°C respectively. For these LCNs, the liquid crystal precursor material was polymerised at 10˚C below the nematic to isotropic transition temperature. It should be noted that these two LCNs have a significantly greater crosslinking density (>20 mol%), and they are used where an extrapolation to 100 mol% mesogenic content is useful in this work.

TABLE I. The composition of the LCEs and LCNs examined in this work. RM82 and A6OCB are acrylate reactive mesogens, whereas EHA is non-mesogenic and MBF is the photoinitiator.

Mesogenic content of Polymerized Material (± 1 mol%)	Composition (mol %)			
	RM82	A6OCB	EHA	MBF
51	6	44	46	3
56	7	49	41	3
60	8	52	37	3
62	8	54	35	3
64	8	56	33	3
65	8	57	32	3
66	8	58	30	4
67	8	59	29	4
70	8	62	27	3
72	9	63	25	4
75	8	67	22	3
98	48	50	0	2
99	22	77	0	2

*Contact author: H.F.Gleeson@leeds.ac.uk

To remain consistent with previous nomenclature [11], a nematic LCE with 62 mol% mesogenic content is referred to in this work as nLCE-62. Several of the LCE films were fabricated with the precursor in the isotropic state, resulting in an isotropic film. In such cases, the samples are denoted as iLCE-XX (where XX indicates the mol% of mesogenic groups). In cases where the LCE film is smectic, it is referred to as sLCE. All LCE films are high-quality monodomain samples, prepared by filling the precursor mixture into a specially prepared mould and polymerising in the appropriate phase (see Supplemental Material [32]).

It is worth noting that the LCE composition of 62 mol% mesogenic content has been widely reported [3-6,8,9,11,21,33], particularly to characterize its auxetic response. Although the auxetic response is not the focus of this work, some of the nematic LCEs discussed in this work also exhibit an auxetic response, details of which are given in the Supplemental Material [32].

B. X-Ray Scattering

For Small- and Wide- Angle X-ray scattering (SAXS and WAXS), small pieces of the LCE films with approximate dimensions of 5 mm x 5 mm and 100 μm in thickness were loaded onto a sample holder and placed into the vacuum chamber of an Anton Paar™ SAXSPoint 5.0. Lanthanum hexaboride (LaB_6) and silver behenate (AgBeh) were used to provide a calibration for WAXS and SAXS, respectively. The setup uses a copper source (1.5418 Å) and the resultant scattering from the sample was detected using an Eiger2 R 1M. All data were collected with three average frames with a count time of 600 seconds each. The temperature of the chamber was measured to be between 28°C and 29°C for all experiments.

The transformation and analysis of SAXS and WAXS data between reciprocal space and real space was performed using the SAXS analysis program by Anton Paar™. To characterize the scattering feature positions and orientations, the scattering intensity data were investigated either radially (φ) or along the azimuthal angle (χ). To measure the location of each feature, Gaussian fits were applied to the peaks of the scattering intensity $I(\varphi)$ in reciprocal space, q (nm^{-1}), then converted to real spacing, d (Å), through $q = \frac{2\pi}{d}$. The uncertainty in the scattering feature position was determined to be 2% through the quality of the Gaussian fitting and repeated measurements of the same material. The correlation length was determined from the SAXS data, providing insight into the ordering within a material. In line with previous methodology used for both main chain and side chain LCEs, the full width half maximum ($w_{\parallel}$) of the Gaussian fitting to the $q \sim 1.5$ nm^{-1} scattering feature was used to measure the correlation length parallel to director ($\xi_{\parallel}$) according to $\xi_{\parallel} = 2\pi/w_{\parallel}$, which is based on the Scherrer equation [10,28,34]. The Gaussian fitting uncertainty in $w_{\parallel}$ provides the uncertainty for the measured correlation length, $\xi_{\parallel}$.

C. Phase Identification

The liquid crystal phase exhibited by each of the LCE systems was determined through a combination of optical microscopy and X-ray scattering. Isotropic films were readily identified from their optical clarity, the fact that they are dark for all orientations when viewed through crossed polarisers and through isotropic X-ray scattering patterns. Nematic and smectic films also exhibited high optical clarity, but their birefringence meant that they were bright when viewed between crossed polarisers with the liquid crystal preferred orientation (director) at 45˚ to the polariser directions. Both nematic and smectic films also show anisotropic X-ray scattering films, with the smectic case distinguished by strong SAXS features and longer correlation lengths.

D. Material Density

Glycerol in water solutions with concentrations between 40 and 80 wt.% in steps of 5 wt.% were prepared and their density, as calculated by Volk and Kähler at specific temperatures, was determined in g/cm^3 [35]. The use of aqueous glycerol solutions allows the density of small, irregular samples of LCEs to be measured to high accuracy (±1%), since the temperature-dependent densities of varied wt.% glycerol solutions are known experimentally to a high precision (±0.01%), and have also been well modelled theoretically (±0.07%) [35,36]. The densities of the LCE films were established *via* their behaviour within a lower and higher wt.% glycerol solution at room temperature (21°C). Each density measurement was repeated to ensure consistent behaviour of the LCE in the solutions. An uncertainty in the LCE density of ± 0.01 g/cm^3 was determined, by considering uncertainties in the temperature and the concentration of the solution. The LCEs exhibited no sign of swelling within the solutions. The densities of the glycerol in water solutions can be accessed in the Supplemental Material [32].

E. Tensile Measurements

The Young's Moduli and Poisson's Ratio of several of the LCEs were measured using a tensile force measurement stage from Instec Inc (HCS350G-TNS). The stage allows the application of a controlled force

*Contact author: H.F.Gleeson@leeds.ac.uk

while measuring the sample length. The sample width was measured using a digital microscope. The initial thickness of the samples was measured with a precision micrometer, and the thickness change during the experiment was calculated assuming volume conservation, a condition known to be characteristic of these elastomer samples [1]. A square-shaped film was used for the measurements, as it enables symmetric characterization in both the longitudinal and transverse directions. The definition of the geometries considered is given in Fig. S6 of the Supplemental Material [32]. For these measurements, samples with mesogenic content of 60 mol%, 65 mol%, 70 mol%, and 75 mol% were used. A similar methodology has been previously used for tensile tests of nLCE-62 [33].

III. RESULTS AND DISCUSSION

A. Phase Assignation

Table II shows the phase assignation of the liquid crystalline LCE films with varying mesogenic content. The limits of the compositional range of this series of materials have been well characterized previously [11,25]; the lowest mesogenic content LCE used (51 mol%) presents as a phase separated nematic material, and the highest mesogenic content materials (98 mol% and 99 mol%) are glassy films at room temperature [25]. For formulations with intermediate mesogenic content, nematic order is confirmed, whereas at concentrations above 70% the films are smectic. Note that isotropic films were fabricated with 67, 72, and 99 mol% of mesogenic content by polymerizing the precursor mixture in the isotropic phase.

B. Density of the LCEs

The materials selected for density measurements are those previously reported for their optical properties so that the expected correlation between refractive index and density could be explored [11]. Two further materials of high mesogenic content (sLCN-98 and iLCN-99) were also investigated. The glass transition temperatures across this series of materials have been previously shown to increase linearly with mesogenic content, with glass transition temperatures rising from ~ 2°C in nLCE-56 to ~57°C in sLCN-98 [11,25]; the linear behaviour of the glass transition data is shown in the Supplemental Material [32].

The density measured at 21°C for these LCEs is shown in Fig. 1 and Table II. An increase in material density, from 1.11 ± 0.01 g/cm^3 to 1.19 ± 0.01 g/cm^3, occurs between the 51 mol% and 99 mol% mesogenic content. This corresponds to a 7% increase in the film density occurring for a large (48 mol%) increase in mesogenic content. The linear trend seen in Fig. 1

TABLE II. The phase assignation of the monodomain nematic, smectic, and isotropic materials between 51 and 99 mol% mesogenic content. The density was measured for selected films at room temperature (21°C), at which sLCN-98 and iLCN-99 are glassy films.

Phase	Name	Mesogenic content (± 1 mol %)	Density (± 0.01 g/cm^3)
Phase separated nematic	nLCE-51	51	1.11
Nematic	nLCE-56	56	1.12
	nCLE-60	60	1.13
	nLCE-62	62	1.13
	nLCE-64	64	1.15
	nLCE-65	65	1.15
	nLCE-66	66	1.15
Smectic	sLCE-70	70	1.15
	sLCE-72	72	1.16
	sLCE-75	75	1.16
	sLCN-98	98	1.19
Isotropic	iLCE-60	60	1.13
	iLCE-62	62	1.13
	iLCE-67	67	1.15
	iLCE-72	72	1.16
	iLCN-99	99	1.19

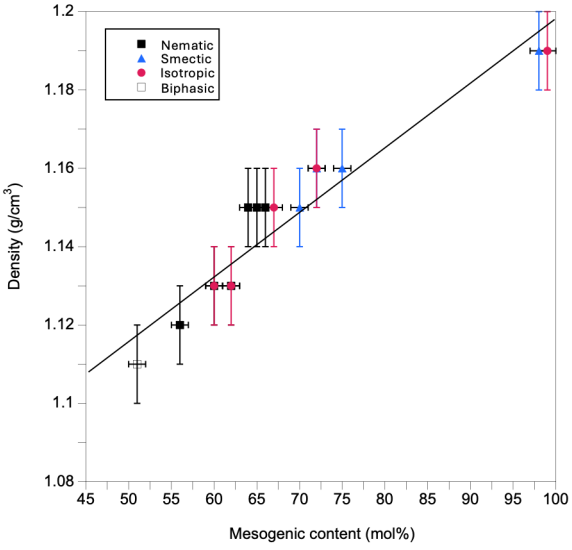

FIG 1. The density of materials templated in the nematic (black squares), smectic (blue triangles), and isotropic (pink circles) phases. A phase separated nematic LCE is also included (empty black square).

*Contact author: H.F.Gleeson@leeds.ac.uk

suggests that the density of the material is controlled by the mesogenic content, with effectively no contribution from the phase or the crosslinker. This conclusion is supported through considering

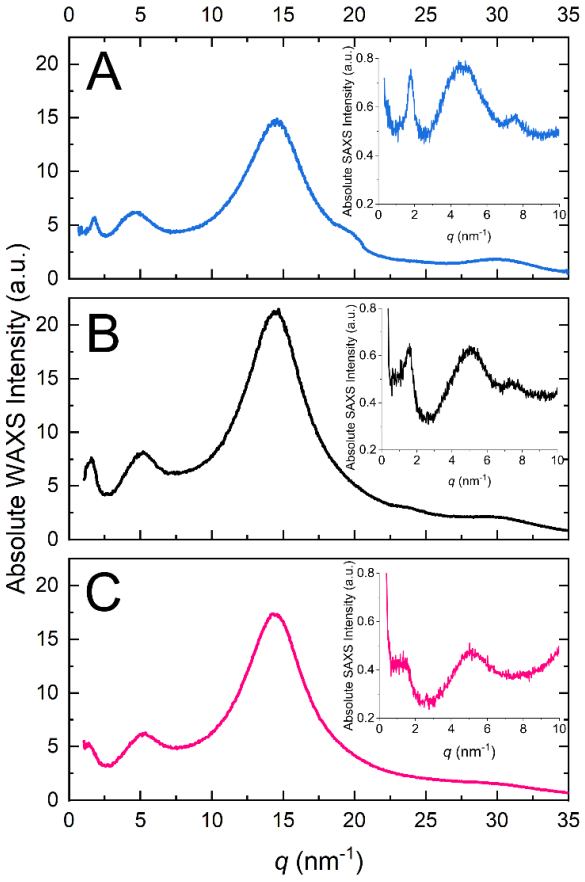

FIG 2. The Wide- and Small- Angle X-ray Scattering intensity from (**A**) sLCE-75, (**B**) nLCE-66, and (**C**) iLCE-67.

chemically identical films fabricated in different states. The two glassy networks of high mesogenic content, sLCN-98 and iLCN-99, have the same density, 1.19 ± 0.01 g/cm^3, even though they have very different crosslink densities (sLCN-98 contains 48 mol% of the crosslinker RM82, while iLCN-99 has only 22 mol%). Further, the densities of sLCE-72 and iLCE-72 are identical, as are those of nLCE-64, nLCE-66, and iLCE-67 (within experimental uncertainty). Clearly, the density of these materials can be selected by the composition and the linear variation seen is in good agreement with the behaviour reported for the average refractive index [11].

C. X-ray Scattering Features and Network Packing

X-ray Scattering allows details of the molecular packing in the LCE films to be explored and compared with the macroscopic measurement of density. This study concentrates on the materials with intermediate mesogen concentration. The phase separated material nLCE-51 is excluded, together with sLCN-98 and iLCN-99, the latter because of their significantly different crosslink densities and the fact that the lack of EHA within the materials results in very different X-ray scattering signals (see figure S3C in the SI).

Fig. 2 presents the SAXS and WAXS intensity for representative smectic, nematic, and isotropic films (see Fig. S4 for all data). The main features are summarised in Table III and representative scattering images are presented in Figs. S2-S4 [32]. Three strong features are observed at $q \sim 1.5$ nm^{-1}, 5 nm^{-1}, and 14 nm^{-1}. For the monodomain nematic and smectic films, the feature at $q \sim 14$ nm^{-1} is perpendicular to the director and corresponds to an average spacing of ~4.4 Å; this can be attributed to the side-to-side spacing of the mesogenic units. The feature at $q \sim 5$ nm^{-1} (~12 Å) is due to the EHA unit. This is inherent to any of the LCE films that contain EHA and presents as a network spacing of 14 Å in poly-EHA (Fig. S3D) [32] and with slightly smaller spacing (~12.5 Å) for the LCEs. The scattering at $q \sim 1.5$ nm^{-1} is attributed to the end-to-end molecular spacing in the LCEs [6]. This feature differs significantly in the smectic, nematic, and isotropic cases, Fig 2. The emergence of smectic order in sLCE-75 can be seen from the pronounced scattering at $q \sim 1.5$ nm^{-1} retaining a Gaussian curve shape even to small q, due to the increased correlation length.

TABLE III. Summary of the scattering features observed using SAXS and WAXS, including their position in reciprocal space (q), their orientation (∥ or ⊥) with respect to the director for monodomain nematic and frustrated smectic LCEs, the strength, and the approximate real spacing that the feature corresponds to. The features at $q \sim 7.4$ nm^{-1} and 23 nm^{-1} only appear for the monodomain nematic and smectic LCEs. Spacings are not calculated for the higher order diffraction features ($q \sim 23$ nm^{-1} and 29 nm^{-1}).

q (nm^{-1})	**Strength**	Approx. **Spacing (Å)**	**Comment**
1.5 (∥)	Strong	45	End-to-end mesogenic spacing
5.0 (∥)	Strong	12	EHA scattering
7.4 (⊥)	Weak	8.5	Only seen in LC films - unclear assignation
14 (⊥)	Strong	4.4	Side-to-side mesogenic spacing
23 (⊥)	Weak		3rd order of 7.4 nm^{-1} feature
29	Weak		2nd order of 14 nm^{-1} feature

*Contact author: H.F.Gleeson@leeds.ac.uk

The variation in the positions of the main scattering features as a function of mesogenic content are presented in Fig. 3. Increasing the mesogenic content results in a reduction in all the spacings, for all phases, Fig. 3A. Over the compositional range investigated, the side-to-side spacing (~4.4 Å) reduces approximately linearly by 2.7% from 4.47 to 4.35 Å for nLCE-56 to sLCE-75, respectively. The spacing corresponding to the EHA feature (~12 Å) shows less obvious monotonic behaviour. Interestingly, the EHA spacing is generally larger in the smectic materials and consistently lower in the isotropic versions (~12.3 Å). However, the greatest change in the network spacing is observed for the end-to-end spacing (~45Å), in which a 22% reduction in the network spacing occurs between nLCE-56 and sLCE-75. Interestingly, a reduction of a similar scale is seen in the isotropic versions of the film, although there is a clear absolute difference between mesogenic and isotropic spacings. The reduction in the network spacing with mesogenic content occurs irrespective of the phase of the material. It is interesting to consider how the change in the network spacings directly influence of the density of these materials, Fig. 3B. As might be expected from the linear dependence of density on mesogenic content, (Fig. 1), Fig. 3A, shows clear reductions in the network spacings for the ~4.4 Å and ~45 Å features. The smectic nature of the LCEs is best seen from the correlation lengths measured parallel to the director, $\xi_{\parallel}$, which are shown with respect to mesogenic content and density respectively in Fig. 3C and Fig. 3D. The correlation length is low for both isotropic films (~60 Å), as would be expected. It increases approximately linearly with mesogenic content in both the nematic (black squares) and smectic LCEs (blue triangles). However, it is the number of 'repeats' that are correlated that gives the most insight to the structures. The nematic LCEs have correlation lengths < 100 Å, less than 2 average end-to-end spacings within the material. Interestingly, the correlation length of the lowest possible mesogenic concentration (before phase separation), nLCE-56 is only slightly higher (63 Å) than in the isotropic LCEs suggesting a minimum correlation length for nematic monodomain LCEs. The smectic materials exhibit the largest correlation lengths, between 125-165 Å, extending over 3-5 smectic layers. Similar compositions of side-chain acrylate LCEs that have been classified as frustrated smectic phases have similar correlation lengths typically extending across less than ~ 5 layers [28]. There is no obvious relationship between correlation length and density (Fig. 3D).

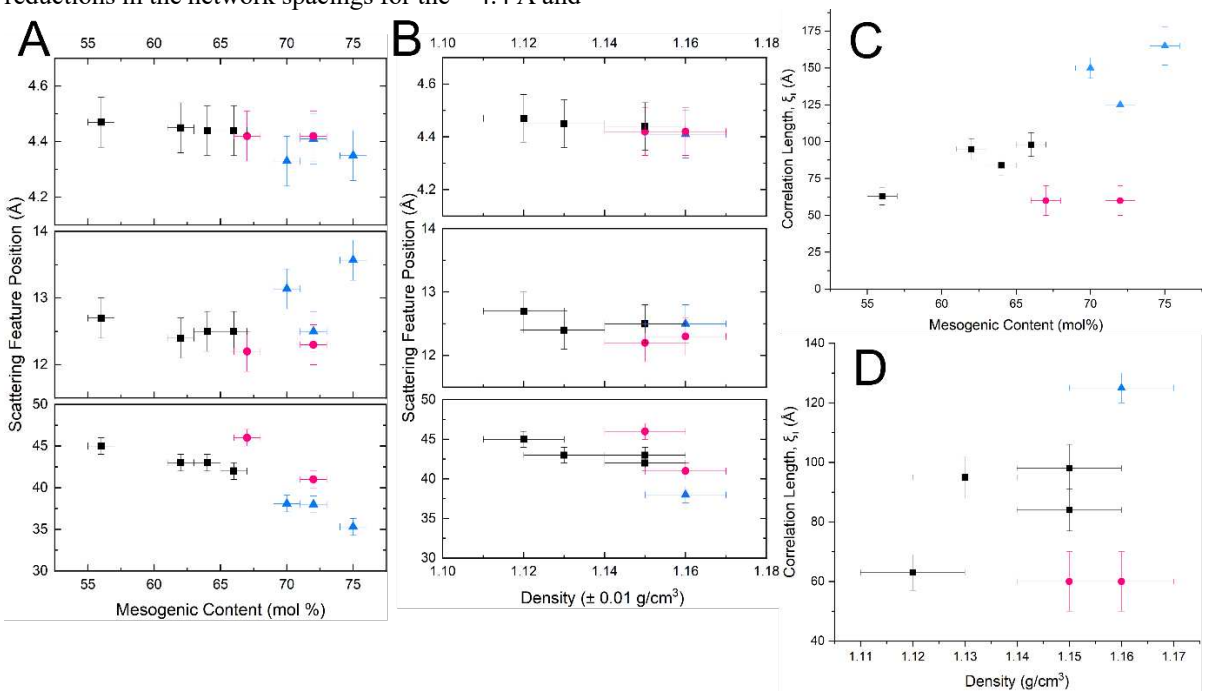

FIG 3. The network spacings measured for side-to-side, EHA-related and end-to-end periodicities (~4.4 Å, ~12 Å, and ~45 Å respectively) for the monodomain nematic (black squares), isotropic (pink circles), and smectic (blue triangles) LCEs, measured a function of (**A**) the mesogenic content and (**B**) the density of the LCE. The correlation lengths parallel to the director, $\xi_{\parallel}$, for monodomain nematic (black squares) and smectic (blue triangles) LCEs as a function of (**C**) mesogenic content and (**D**) the density of the LCE, with the correlation lengths of the isotropic LCEs (pink circles) also included.

*Contact author: H.F.Gleeson@leeds.ac.uk

D. The Moduli and Poisson's Ratio of the LCEs

This series of LCEs offers an opportunity to study the mechanical properties such as Young's moduli and Poisson's ratios with respect to subtle and continuous changes in packing and ordering. The Young's moduli measured parallel and perpendicular to the director are detailed in Fig. 4A at 21˚C; a comparison between data at 18 ˚C and 21˚C is in Fig. S8 in the Supplemental Material [32]. In the perpendicular case, the moduli are approximately constant for the materials with concentrations ≤ 70 mol%, increasing by a factor of ~3 for sLCE-75. The parallel case is similar, though there is a significant increase in the Young's modulus for both sLCE-70 and sLCE-75, which show ~ 40% and ~ 85% greater moduli respectively than the systems with lower mesogenic concentration. Such an observation is in keeping with the expectation that deformations that require a change in smectic layer spacing are hindered. However, the large changes in sLCE-75 could also be in part due to the proximity of the glass transition. Using the linear fit to the glass transition temperatures of this family of materials (Fig. S5 of Supplemental Material) [32], the glass transition is expected to occur around room temperature for sLCE-75 (~ 23°C) [11,25,37].

The former explanation is considered to dominate as the moduli of the frustrated smectic material sLCE-75 are in close agreement to other well-characterized frustrated smectic LCEs; for example, a chemically similar material with a longer spacer length on the side-group (A7OCB as a replacement to A6OCB), has been previously reported to have Young's moduli of 16.5 MPa and 2.8 MPa parallel and perpendicular to the director, respectively [28]. In the case of sLCE-70, we see moduli with values between the nematic materials and sLCE-75, reflecting that this material has the minimum concentration required to form a frustrated smectic phase, 70 mol% mesogenic content.

As already mentioned, the nematic templated LCEs show negative Poisson's ratios when strained beyond threshold strains, which were measured to be between 0.49 ± 0.05 and 0.63 ± 0.05 for nLCE-62 and nLCE-66 (Fig. S1 in Supplemental Material) [32]. Although it has recently been shown that some frustrated smectic LCEs can also show auxetic behaviour if they can be strained beyond their threshold [10], in the present work we focused on low strains within the linear elastic regime (~0.1). Fig. 4B shows the Poisson's ratios for different concentrations of mesogenic content when the applied stress is along the z axis parallel to the director (Fig. S6A in Supplemental Material) [32] and measured at 21˚C. Theoretically, for a medium with volume conservation during the deformations, the values of $\sigma_{\parallel x}$ and $\sigma_{\parallel y}$ should be equal to 0.5 which is close to the average seen for this system, 0.47 ±0.01. The small deviation of the experimental values from theory may be due to small errors in the direction of force application (even a small inaccuracy can lead to such a deviation). There is also strong anisotropy in the Poisson's ratio which, in the case of sLCE-75, is slightly larger than in the nematic case. Such behaviour may be attributed to a transition from the nematic to a frustrated smectic phase, where anisotropy between the orthogonal axes is enhanced by the constraints of the layered structure. We know of no theoretical calculations of the Poisson's ratio in frustrated smectic structures such as those considered here, so further comparison with theoretical predictions is not possible.

In general, polarized optical microscopy provides information about the liquid crystal phase and qualitative insight into the director orientation. However, in the case of planar alignment, the images are identical for two orthogonal directions. Therefore, since the Young's modulus and Poisson's ratio differ significantly when tensile tests are performed parallel and perpendicular to the director, mechanical measurements can serve as an additional tool for identifying the director orientation.

IV. CONCLUSIONS

This work furthers the understanding of the packing and the structure of chemically similar LCEs, showing that the network spacing changes uniformly across a series of monodomain nematic, smectic, and isotropic LCEs. The general reduction in the network spacings that is observed with increasing mesogenic content, and the associated closer packing is reflected by an increase in the material density. Using aqueous glycerol solutions, the densities of materials between 51 mol% and 99 mol% mesogenic content were measured to vary from 1.11 ± 0.01 g/cm^3 to 1.19 ± 0.01 g/cm^3. This is a 7% increase in the density for a 48% increase in the mesogenic content. Considering both the mesogenic and isotropic versions of the elastomers has allowed us to conclude that the density is independent of the phase and can be controlled by the mesogenic content alone. This direct finding regarding the density supports the previous observation that for these materials the average refractive index of a monodomain nematic LCE is identical to its isotropic analogue and that there is a linear dependence of both on concentration [11].

A concentration-related transition between monodomain nematic and frustrated smectic LCEs has also been demonstrated. For the 70 mol% mesogenic content material (sLCE-70) a smectic layer spacing of~ 38 Å and correlation length of 150 Å (~ 4 layers)

*Contact author: H.F.Gleeson@leeds.ac.uk

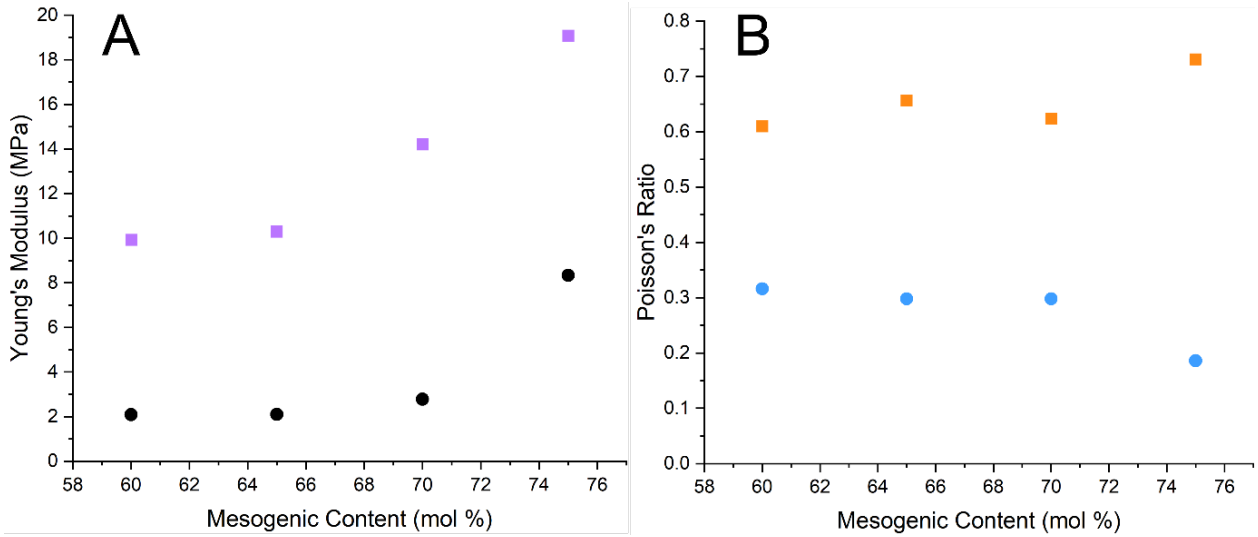

FIG 4. (**A**) The Young's Moduli measured for LCEs between 60 mol% and 75 mol% mesogenic content, with the applied stress parallel (purple squares) and perpendicular (black circles) to the director. (**B**) The Poisson's ratios for different concentrations of mesogenic content when the applied stress is along the z axis and parallel to the director (defined in the Supplemental Material [32]). The blue circles and orange squares represent $\sigma_{\parallel x}$ and $\sigma_{\parallel y}$ respectively. All measurements were taken at 21°C.

allows the material to be classified as a frustrated smectic in accordance with the work of Berrow *et al*. [28]. Such X-ray scattering analysis is critical for distinguishing between nematic and frustrated smectic LCEs which have very different bulk properties. Previously, sLCE-72 was considered to be nematic because of the linear variation in optical parameters between it and the known nematic analogues with slightly lower mesogenic concentrations [11]. However, here we have demonstrated that materials above 70 mol% mesogenic content possess a frustrated smectic nature. Excitingly, this elucidates that frustrated smectic materials can also be optically tuned following the compositional design rules that have been previously outlined [11].

The mechanical properties of this family of materials show a clear evolution from nematic to frustrated smectic LCEs and across the nematic-glass transition temperature. The changes in Young's moduli and the Poisson's ratio can provide additional insight into the order, phase, and director orientation of LCEs. It is known that in the smectic phase of a liquid crystal [38,39], spatial distortions perpendicular to the layers are very small, similar to those in a solid, whereas relative displacements within the layer plane encounter weak resistance, often weaker than in the nematic phase. Consequently, when the material is stretched along a direction lying in the plane of the smectic layers, the deformation along the in-plane direction y is greater than in the nematic phase, while the deformation along the perpendicular direction x is smaller. Accordingly, the Poisson's ratio $\sigma_{\parallel y}$ becomes larger than in the nematic phase, whereas $\sigma_{\parallel x}$ becomes smaller. In our case, because increasing the mesogenic content induces a transition from the nematic to the frustrated smectic phase, we observe an increase in $\sigma_{\parallel y}$ and a decrease in $\sigma_{\parallel x}$.

A full comprehension of the composition-dependent material properties is critical for selecting the ideal material for an application. The monodomain nematic materials within this family are strongly associated with a unique auxetic response to strain, which is critical to the proposed applications of these materials as laminates in impact resistant glass. Whilst investigating the tuneable properties of LCEs here, we have shown that monodomain nematic LCEs of different compositions can retain an auxetic behaviour. When polymerized at room temperature, the ordering and anisotropy of these LCEs are known to be controllable *via* the mesogenic content [11], and this paper has established that a fine control of the material properties is possible to the nanoscale. Here, we have reported changes to the network packing and the density across a series of varied composition LCEs which allows a deep insight into the control of both phase and material properties. Specifically, fine control of the optical properties, density, and mechanical properties of these LCEs suggests that

*Contact author: H.F.Gleeson@leeds.ac.uk

lightweight optical applications are especially appropriate for them. Alongside the known unique auxetic capabilities of the nematic variants, applications for these materials extends across optical elements, wearable sensors, and impact resistance glass.

ACKNOWLEDGEMENTS

E.C, S.R.R., T.R, D.M and H.F.G thank the Engineering and Physical Sciences Research Council of Great Britain under the research grant EP/V054724/1, and the grant EP/X0348011 for the purchase of the Anton Paar SAXSPoint 5.0 which is used in this work. E.J.C. is grateful for support by the Engineering and Physical Sciences Research Council of Great Britain under the research grant EP/T517860/1. The work of K.M., G.G., M.H., and R.H. was supported by the Higher Education and Science Committee of the RA in the frames of research project 21AG-1C088. D.M. thanks the Leverhulme Trust for an Early Career Fellowship. E.I.L.J. thanks the Northern Triangle Initiative for funding.

DATA AVAILABILITY

The dataset associated with this work can be accessed at reference 41.

AUTHOR CONTRIBUTIONS

Conceptualization: E.J.C. and H.F.G.; Data curation: E.J.C., S.R.B., K.M., G.G., T.R.; Formal analysis: E.J.C., S.R.B., G.G., R.H., T.R.; Funding acquisition: D.M., G.G., R.H., H.F.G.; Investigation: E.J.C, S.R.B., K.M., G.G., M.H., T.R., D.M.; Methodology: E.J.C, S.R.B., G.G., T.R., D.M.; Project administration: E.J.C. and H.F.G.; Resources: E.J.C., S.R.B., G.G, E.I.L.J.; Software: E.J.C., S.R.B., T.R.; Supervision: D.M., P.H., R.H., H.F.G.; Validation: E.J.C., S.R.B., G.G., R.H., T.R.; Visualization: E.J.C., G.G., M.H., H.F.G.; Writing – original draft: E.J.C. and H.F.G.; Writing – review & editing: E.J.C. S.R.B., G.G., T.R., P.H., R.H., H.F.G.

REFERENCES

[1] D. Mistry, S. D. Connell, S. L. Mickthwaite, P. B. Morgan, J. H. Clamp, and H. F. Gleeson, Nat. Commun. **9**, 5095 (2018).
[2] D. Mistry, P. B. Morgan, J. H. Clamp, and H. F. Gleeson, Soft Matter **14**, 1301 (2018).
[3] Z. Wang, T. Raistrick, A. Street, M. Reynolds, Y. Liu, and H. F. Gleeson, Materials **16** (2022).
[4] S. R. Berrow, R. J. Mandle, T. Raistrick, M. Reynolds, and H. F. Gleeson, Macromolecules **57**, 5218 (2024).
[5] T. Moorhouse and T. Raistrick, Adv. Opt. Mater. **12**, 2400866 (2024).
[6] S. R. Berrow, T. Raistrick, R. J. Mandle, and H. F. Gleeson, Polymers (Basel) **16**, 1957 (2024).
[7] S. R. Berrow, T. Raistrick, R. J. Mandle, and H. F. Gleeson, ACS Appl. Polym. Mater. **7**, 4517 (2025).
[8] T. Raistrick, M. Reynolds, E. J. Cooper, J. Hobbs, V. Reshetnyak, and H. F. Gleeson, Soft Matter **21**, 8849 (2025).
[9] Z. Wang, T. Raistrick, M. Cheng, E. J. Cooper, M. Reynolds, M. Cen, H. F. Gleeson, and Y. J. Liu, Mater. Horiz. **Advance Article** (2026).
[10] A. Street, S.R. Berrow, Z. Wang, E.J. Cooper, J. Mattsson, and H. F. Gleeson, Research Square [Preprint] (2026).
[11] E. J. Cooper, M. Reynolds, T. Raistrick, S. R. Berrow, E. I. L. Jull, V. Reshetnyak, D. Mistry, and H. F. Gleeson, Macromolecules **57**, 2030 (2024).
[12] Q. He, Z. Wang, Z. Song, and S. Cai, Adv. Mater. Technol. **4**, 1800244 (2019).
[13] D. Sun, J. Zhang, H. Li, Z. Shi, Q. Meng, S. Liu, J. Chen, and X. Liu, Polymers **13** (2021).
[14] M. Camacho-Lopez, H. Finkelmann, P. Palffy-Muhoray, and M. Shelley, Nat. Mater. **3**, 307 (2004).
[15] A. Sharma *et al.*, Macromol. Biosci. **15**, 200 (2015).
[16] T. Bera, C. Malcuit, R. J. Clements, and E. Hegmann, Front. Mater. **3** (2016).
[17] M. Hussain, E. I. L. Jull, R. J. Mandle, T. Raistrick, P. J. Hine, and H. F. Gleeson, Nanomaterials **11**, 813 (2021).
[18] D. Mistry, M. Nikkhou, T. Raistrick, M. Hussain, E. I. L. Jull, D. L. Baker, and H. F. Gleeson, Macromolecules **53**, 3709 (2020).
[19] L. Li, H. Bai, X. Dong, Y. Jiang, Q. Li, Q. Wang, N. Yuan, and J. Ding, Langmuir **39**, 12412 (2023).
[20] T. Ohzono, M. O. Saed, and E. M. Terentjev, Adv. Mater. **31**, 1902642 (2019).
[21] A. Street, D. Mistry, J. Mattsson, and H. F. Gleeson, Adv. Funct. Mater., e22644 (2025).
[22] H. Finkelmann, H.-J. Kock, and G. Rehage, Makromol. Chem., Rapid Commun. **2**, 317 (1981).
[23] Y.-G. Jia, B.-Y. Zhang, M. Tian, and W. Pan, J. Appl. Polym. Sci. **93**, 1736 (2004).
[24] G. Cordoyiannis, A. Lebar, B. Zalar, S. Žumer, H. Finkelmann, and Z. Kutnjak, Phys. Rev. Lett. **99**, 197801 (2007).

*Contact author: H.F.Gleeson@leeds.ac.uk

[25] E. I. L. Jull, R. J. Mandle, T. Raistrick, Z. Zhang, P. J. Hine, and H. F. Gleeson, Macromolecules **55**, 4320 (2022).
[26] M. Barnes, S. Cetinkaya, A. Ajnsztajn, and R. Verduzco, Soft Matter **18**, 5074 (2022).
[27] A. R. Tajbakhsh and E. M. Terentjev, Eur. Phys. J. E. **6**, 181 (2001).
[28] S. R. Berrow, T. Raistrick, A. Street, E. J. Cooper, M. Coleman, R. J. Mandle, and H. F. Gleeson, J. Mater. Chem. C **13**, 12365 (2025).
[29] D. Liu, C. W. M. Bastiaansen, J. M. J. den Toonder, and D. J. Broer, Macromolecules **45**, 8005 (2012).
[30] D. Liu and D. J. Broer, Nat. Commun. **6**, 8334 (2015).
[31] J. C. R. Reis, I. M. S. Lampreia, Â. F. S. Santos, M. L. C. J. Moita, and G. Douhéret, ChemPhysChem **11**, 3722 (2010).
[32] See Supplemental Material [url] for details on the Material Synthesis, Auxetic Response, Density of Glycerol Solutions, X-ray Scattering, Glass Transition Temperature, and Tensile Measurements, which includes Refs. [1-11,25,33,35,37].
[33] G. S. Gevorgyan, M. L. Sargsyan, M. R. Hakobyan, M. Reynolds, H. F. Gleeson, and R. S. Hakobyan, Polymers **17**, 614 (2025).
[34] D. T. Kennedy, J. D. Hoang, M. F. Toney, and T. J. White, Macromolecules **57** (2024).
[35] A. Volk and C. J. Kähler, Exp. Fluids **59**, 75 (2018).
[36] L. W. Bosart and A. O. Snoddy, Ind. Eng. Chem. **20**, 1377 (1928).
[37] D. J. Haloi, S. Roy, and N. K. Singha, J. Polym. Sci., Part A: Polym. Chem. **47**, 6526 (2009).
[38] L. D. Landau and E. M. Lifshitz, *Theory of Elasticity* (Butterworth-Heinemann, Oxford, 1986), Theory of Elasticity (Third Edition).
[39] S. Fujii, S. Komura, and C.-Y. D. Lu, Materials **7**, 5146 (2014).
[40] P. G. de Gennes, *Phys. Lett.* **28A**, 725 (1969)
[41] Data are available at https://doi.org/10.5518/1822.

*Contact author: H.F.Gleeson@leeds.ac.uk

*Contact author: H.F.Gleeson@leeds.ac.uk